A reliable acoustic path: Physical properties and a source localization method*

Duan Rui(段 睿), Yang Kun-De(杨坤德)†, Ma Yuan-Liang(马远良), and Lei Bo(雷 波)

College of Marine, Northwestern Polytechnical University, Xi'an 710072, *China*

(Received 22 March 2012; revised manuscript received 12 June 2012)

The physical properties of a reliable acoustic path (RAP) are analysed and subsequently a weighted-subspace-fitting matched field (WSF-MF) method for passive localization is presented by exploiting the properties of the RAP environment. The RAP is an important acoustic duct in the deep ocean, which occurs when the receiver is placed near the bottom where the sound velocity exceeds the maximum sound velocity in the vicinity of the surface. It is found that in the RAP environment the transmission loss is rather low and no blind zone of surveillance exists in a medium range. The ray theory is used to explain these phenomena. Furthermore, the analysis of the arrival structures shows that the source localization method based on arrival angle is feasible in this environment. However, the conventional methods suffer from the complicated and inaccurate estimation of the arrival angle. In this paper, a straightforward WSF-MF method is derived to exploit the information about the arrival angles indirectly. The method is to minimize the distance between the signal subspace and the spanned space by the array manifold in a finite range-depth space rather than the arrival-angle space. Simulations are performed to demonstrate the features of the method, and the results are explained by the arrival structures in the RAP environment.

Keywords: reliable acoustic path, multipath arrival structure, source localization

PACS: 43.30.Cq, 43.30.Wi **DOI:** 10.1088/1674-1056/21/12/124301

1. Introduction

Besides the surface duct and the deep sound channel, the reliable acoustic path (RAP) is the third acoustic duct for sound propagation in the deep ocean. The RAP conditions occur when the receiver is placed at the deep ocean where the sound velocity exceeds the maximum sound velocity in the vicinity of the surface. The depth where this occurs is referred to as the critical depth. A typical example and the corresponding RAPs are shown in Fig. 1. The concept of the RAP has been proposed for many decades, but until recent years many workers began to analyze the properties and the application of the RAP. The ONR-sponsored Philippine Sea experiment is a three-year basic research on deep water ocean acoustics. One of the objectives of the experiment was to examine the multipath structure of RAP propagation at the seafloor.[1−3] A full water-column-spanning distributed vertical line array (DVLA) of 5000-m length makes it possible to give the noise spectrum and obtain the arrival structures on the receivers near the seafloor. The RAP environment provides a high signal-to-noise ratio (SNR) environment for source localization. First, the RAP is the direct path between the source and receiver and thus it is insensitive to the surface scattering and the bottom reflection loss. The transmission loss (TL) corresponding to the RAP is much lower than that corresponding to other paths (e.g., surface reflected path).[4] Second, the ambient noise accompanying the RAP is much lower than the average ambient noise in the deep ocean. It was presented by Gaul *et al.*[5] that under beginning surface conditions the ambient noise of low frequency (below 200 Hz) below the critical depth was about 20-dB lower than that above the critical depth. This phenomenon stems from the fact that the distant shipping (beyond 200 km) noise cannot penetrate to the depth below the critical depth according to Snell's law. For a source within a certain range of the acoustic array placed near the sea bottom, it can be detected by taking advantage of the RAP. Westwood[6]

*Project supported by the National Natural Science Foundation of China (Grant Nos. 11174235 and 61101192), the Science and Technology Development Project of Shaanxi Province, China (Grant No. 2010KJXX-02), the Program for New Century Excellent Talents in University, China (Grant No. NCET-08-0455), the Foundation of State Key Lab of Acoustics, China (Grant No. SKLOA201101), and the Doctorate Foundation of Northwestern Polytechnical University, China (Grant No. CX201226).

†Corresponding author. E-mail: ykdzym@nwpu.edu.cn

© 2012 Chinese Physical Society and IOP Publishing Ltd

concluded that the localization performance would be better when there were arrivals of RAP on the array. Heaney *et al.*[3] also illustrated the advantages of the RAP for matched-field localization using the data recorded on a 5000-m depth array in the Philippine Sea 2009 experiment. Although the RAP environment is good for source localization, little work dealt with the analysis of its acoustic properties in detail. Thompson[7] has analysed the influences of ocean depth and sound frequency on the sound field in the RAP environment. However, the properties determining the performance of the source localization, such as normal modes and the arrival structures, were not presented in the paper. The present paper focuses on the analysis of the arrival structures to provide the theoretical basis for the source localization method. It is shown that the properties of arrival structures determine the feasibility and the performance of the source localization method based on the ray theory.

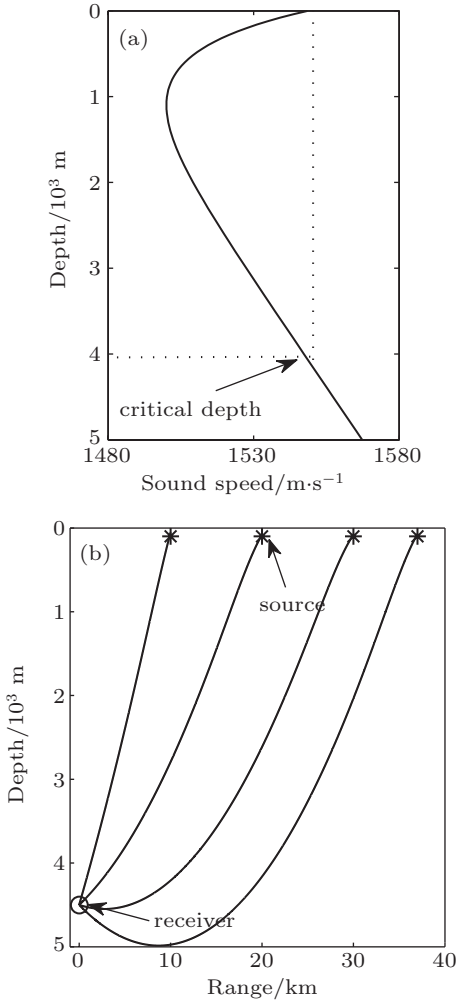


Fig. 1. Illustration of the reliable acoustic path. (a) Sound speed profile as a function of depth, showing that the critical depth is the depth where the sound speed is the same as that at the ocean surface. (b) Reliable acoustic paths from shallow sources to a deep receiver.

As the RAP environment has its own acoustic properties, the general source localization method is not effective in this environment. The matched-field processing (MFP) is a popular method for source localization in shallow water.[8,9] However, for matched-field localization, the array aperture is generally comparable to the ocean depth to provide a unique representation of each propagating mode, which imposes a severe limitation on its application in the deep ocean.[10−13] An alternative method is to increase the signal bandwidth for improving performance.[14] For an array with a small aperture detecting the narrowband signal (line spectrum of a source), the arrival angle and/or delay structure of multipath arrival are utilized to accomplish the source localization.[15−20] In general, two techniques are applied. The first one is to back propagate the rays, in which the source location is determined by the convergence of the rays, and the second one is to compare the measured arrival structures with those calculated from a hypothesized source position, and the source location is determined by the smallest difference. It is the feature matching method. The first step of the two methods is to estimate the arrival structure, including the direction of arrival (DOA) or time delay of arrival (TDOA). In general, the DOAs of the eigenrays can be very close to each other and thus the high-resolution method must be adopted. In some cases, the multiple signal classification (MUSIC) method is unable to distinguish these DOAs[17] and the time-exhausting methods with higher resolution such as the maximum likehood (ML), the weighted subspace fitting (WSF)[21] must be used. These methods are solved by iteration and are sensitive to the initial parameters.[21] The results may be unreliable for the convergence to the local minimum values. Above all, the ray backpropagation and feature matching methods are difficult to use in practice. In this paper, based on the acoustic properties of the RAP environment a weighted-subspace-fitting matched-field (WSF-MF) method for source localization is presented to shorten the array aperture greatly. At the same time the complicated and inaccurate estimation of multipath arrival structures is avoided.

The rest of this paper is organized as follows. In Section 2 the acoustic properties of the reliable acoustic path are analysed. In Section 3, the WSF-MF method for passive source localization is derived in detail. In Section 4, simulations of source localization are performed to evaluate the performance of the

WSF-MF method. The properties of the RAP environment and the localization method are summarized in Section 5.

2. Physical properties of RAP environment

2.1. Shadow zone

The sound in the deep ocean is characterized by long-range propagation for the features of acoustic ducts, which are the surface duct (SD) and the deep sound channel (DSC). However, long-range propagation always suffers from the shadow zone, which results in unreliability of the target surveillance in a medium range. The reliable acoustic path (RAP), though it cannot realize long-range propagation, does not have a shadow zone in the medium range, which contributes to its application for target surveillance.

In the SD, where temperature and salinity are nearly constant, sound speed increases with pressure and thus a positive sound speed gradient is formed. The sound tends to be "trapped" in the surface duct and therefore is attenuated by cylindrical spreading. However, as the SD is homogenized by active turbulence generated by the air–sea interchange, the spatiotemporal variations of the SD are remarkable. Therefore, the SD is unstable. The DSC is at the depth where the minimum velocity is found. From the ocean surface to this depth, the sound speed gradient is negative for the decrease of the temperature while from this depth to the bottom, the sound speed gradient is positive, which is caused by the increase of the hydrostatic pressure. According to Snell's law, the sound would propagate around the DSC without reflections from the surface and the bottom. The DSC has a typical depth at 1000 m, where the water properties are much more persistent than the water in the upper ocean. Therefore, the DSC is stable. Transmission loss (TL) as an example of the SD calculated by the ray approach is shown in Fig. 2(a), where the source is placed at a depth of 50-m. The acoustic environment contains the SD of 120 m. In the SD, the TL at 60 km in range is fairly low (about 7 dB) indicating the good feature for trapping sound of the SD. However, a shadow zone with high TL (about 100 dB) is obvious below the SD which imposes a great restriction on the use of target surveillance. In a static environment, the acoustic reciprocity indicates that acoustic propagation is bidirectional; thus in terms of the square law (energy) detector, if the detector is placed in the SD the target in the SD can be detected much more easily than the target in the shadow zone. When the source is placed at the DSC axis (100 m), the TL is shown in Fig. 2(b). In the range beyond 40 km, the zone around DSC with low TL indicates that the main feature of the DSC is that the sound energy is trapped around the channel. However, the shadow zone between 10 km to 40 km in range indicates that the DSC is not suitable for target surveillance in the medium range. According to the acoustic reciprocity, placing the detector near the DSC is also not effective for the target detection in the medium range.

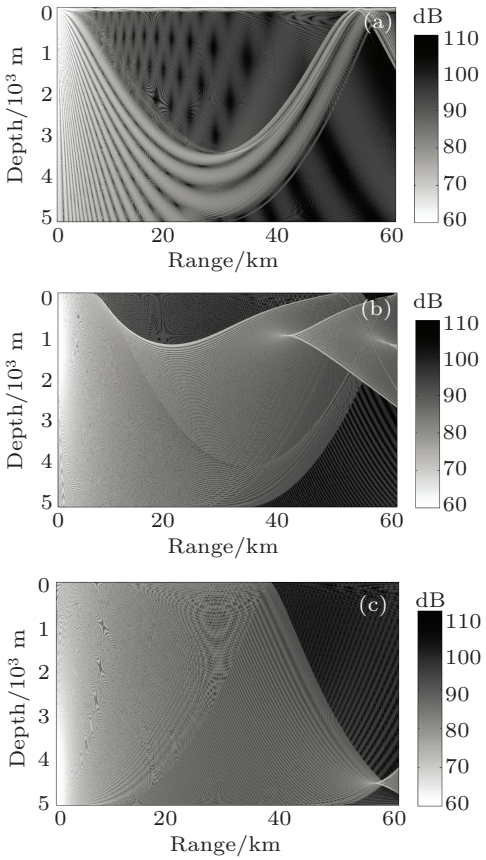


Fig. 2. Sound fields in the deep ocean in three cases, when the source is placed (a) 50 m in the 112-m surface duct, (b) in the deep sound channel, and (c) 4500 m below the critical depth.

When the source is placed at 4500-m depth, the sound field in Fig. 2(c) does not have shadow zones in the medium range (within 40 km) and the low TL zone is bowl-shaped if the sound field is presented in three-dimensional (3D) space. The bowl-shaped zone is the main feature of the RAP environment. It is estimated that the radius of the surface coverage of this zone is approximately eight times the water depth. For the direct arrival from the source to the receiver, the TL in

this zone is relatively low. Outside this zone, no direct path arrives at the receiver and the sound suffers from loss of reflection and scattering on the surface and the bottom. Therefore, the transmission loss is high. For acoustic reciprocity, a detector near the bottom can detect the surface target and the submerged target in the medium range without any blind zone. It must be pointed out that the RAP environment cannot be used for long-range detection or communication as the sound outside the bowl-shaped zone interacts with the boundaries and attenuates quickly.

2.2. Acoustic propagation in the RAP environment

The conventional matched-field methods require an array aperture comparable to the ocean depth according to the normal mode theory. As this work tries to use a short array to localize a source based on the ray arrival structure, the ray theory is used to analyse the acoustic propagation that occurs in the RAP environment.

2.2.1. Propagation path

The eigenrays from a source at a depth of 210 m to a receiver at a depth of 4450 m are shown in Fig. 3. Five horizontal ranges of the source are assumed to be 5, 20, 30, 37, and 40 km, respectively. At each range only those eigenrays within 10 dB of the strongest are shown. The eigenrays are colour coded by their normalized amplitudes on the receiver. The environment is range-independent. The sound speed profile (SSP) following a Munk profile is shown in Fig. 1(a). The medium is terminated with a homogeneous half-space with a sound speed of 1650 m/s. The density is 1800 kg/m^3 and the attenuation coefficient is 0.5 dB/λ, where λ denotes the wavelength. The rays penetrating into the bottom are neglected, so the acoustic properties of the half-space are chosen to simulate the sediment layer in the deep ocean. The frequency for the simulation is 30 Hz.

At the shortest range of 5 km, only the direct (D) and the surface-reflected (S) rays are significant. At the short range, rays penetrate into the bottom with large grazing angles and thus major energy is attenuated in the substrate. When the source is placed at 20 km in range, besides the D and S rays, the bottom-reflected (B) and the surface-bottom reflected (SB) rays become significant. As the rays penetrate into the bottom with smaller grazing angles, more energy is reflected into the water. The bottom-surface reflected (BS) ray is weak due to the large grazing angle on the bottom and the additional geometric attenuation. For the source at 30-km range, two new types of rays become significant. The D, S, and SB rays are strongly bent, indicating that they are close to being cut off by the gradient of the SSP. Therefore, at a range of 37 m, the three types of rays are cut off and the B ray exhibits strong bending. To a range of 40 km, the B ray is also cut off and only the rays with two or more bounces between the boundaries can arrive at the receiver.

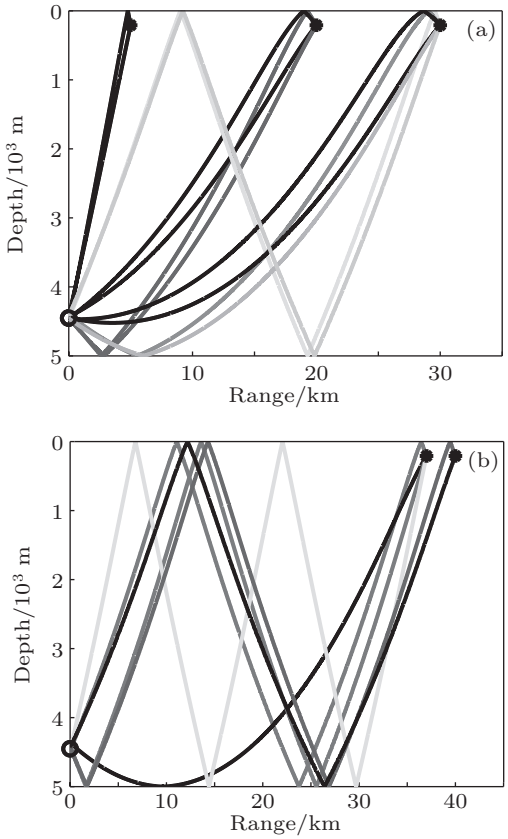


Fig. 3. Eigenrays from a source at a depth of 210 m to a receiver at a depth of 4450 m at (a) horizontal ranges of 5, 20, and 30 km, and horizontal ranges of 37 km and 40 km (b).

2.2.2. Arrival structure

The arrival angles and the time delays of multipath arrivals are the most important properties of a source-receiver configuration. The analysis of the arrival structures changing with source-receiver configuration is important for knowing the feasibility of the ray-based localization method. In the RAP environment where the receiver is near the bottom while the source is near the surface, the arrival structure has special properties. The arrival structure on a receiver

of 4450 m in depth along with a source of 210 m in depth and 30 km in range is shown in Fig. 4. Five groups of arrivals with time intervals from two to six seconds are clearly identified. The time intervals correspond to the propagation time between the surface and the bottom. In the first group, four arrivals are D, B, S, and SB arrivals in the order of arrival time. For the other groups, the arrivals suffer more scattering losses caused by the surface and the bottom reflection. Therefore, these arrivals are weak and unstable. As the D, B, and S arrivals are the strongest and most stable arrivals, the localization method based on these arrivals can be robust. Therefore, the properties of these arrivals are analysed in the following.

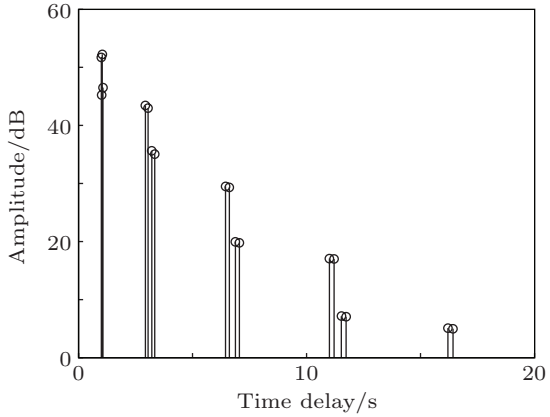


Fig. 4. The arrival structure on a receiver of 4450 m in depth along with a source of 210 m in depth and 30 km in range.

Firstly, the arrival angles on a near-bottom receiver changing with source location are examined. In the following, the simulations are focused on the region from 5 km to 40 km in range and 0 m to 1200 m in depth. Figure 5 displays the arrival angles of D (a), S (b), and B (c) arrivals on a receiver of 4450 m in depth. The units are degrees and the degree intervals between adjacent contours are two degrees. Three important features of the arrival angles in the RAP environment are as follows.

1) Firstly the contours for a certain type of arrivals are oriented in the same directions. The orientation of the contours for the S arrival is different from those of the other two, which indicates that the sources can be distinguished in the depth direction. Otherwise, false sources will appear along the contour where the real source is located.

2) Secondly, the contours become denser and steeper with the decrease of the range. It demonstrates that the resolution in the range direction increases with the decrease of the range. Besides, the calculation results illustrate that the decreasing (D arrival) or the increasing (S and B arrivals) rates of the arrival angles in the depth direction also increase with the decrease of the range. Therefore, if a method is valid in the far region, it can also be valid in the near region.

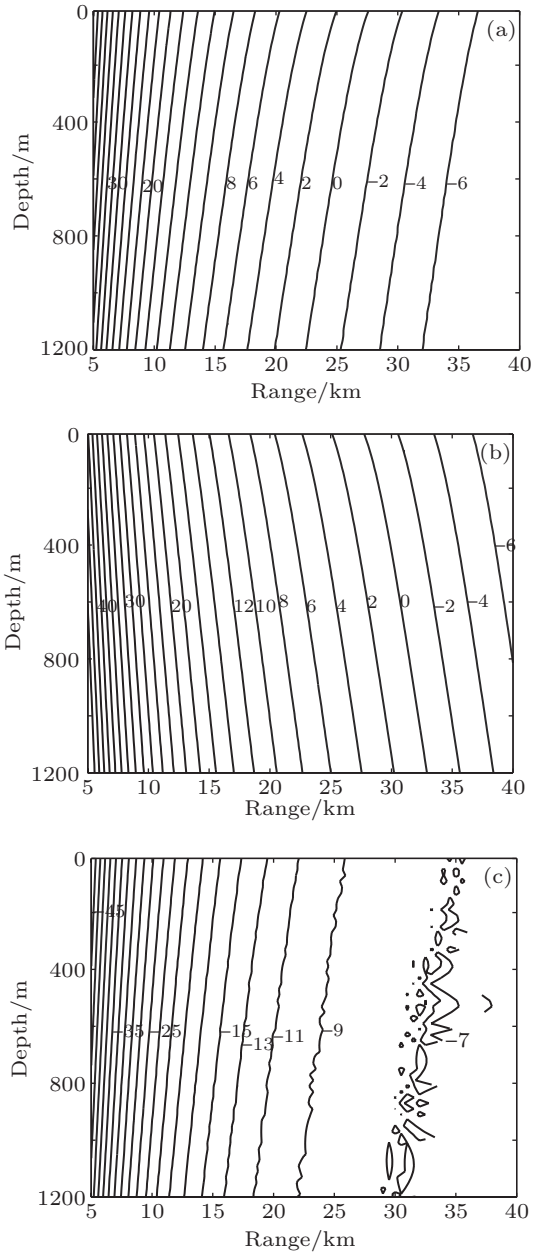


Fig. 5. Contours of arrival angles on a receiver at 4450-m deep for the cases of (a) direct arrival, (b) surface-reflected arrival, and (c) bottom-reflected arrival .

3) Thirdly, figure 5 shows that the arrival angles of the three arrivals are much more sensitive to the range than to the depth. As a result, the resolution in the range direction is higher than that in the depth direction. Figure 6(a) shows the arrival angles changing with source range (from 20 km to 40 km) when the

source is at 210-m deep. As the arrival angle is sensitive to the range it is anticipated that if the source depth has been known the range is easy to determine. Figure 6(b) illustrates the sensitivity of the arrival angle to the source depth when the source is at 30 km in range. The arrival angle, especially the B arrival angle, is more insensitive to the source depth than to the source range. As a result, the source localization method based on the arrival angle can be effective to determine the range but not the depth of the source. Several examples can be seen in Section 4.

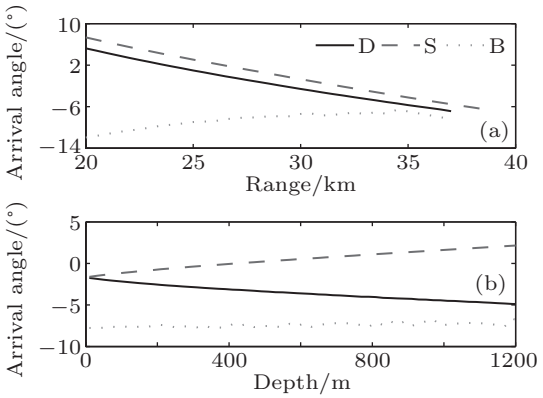


Fig. 6. Variations of arrival angles on a receiver at 4450-m depth with source location for the cases, i.e., when (a) the source depth is fixed to be 210 m, and (b) the source range is fixed to be 30 km.

For the source localization method based on the arrival time, the time delay relative to the D arrival is important. The time delays of S and B arrivals relative to the D arrival on a receiver of 4450-m deep are shown in Figs. 7(a) and 7(b), respectively. The time delay of S arrival is very sensitive to the source depth but insensitive to the source range when the range is beyond 20 km. In the region within 20 km, the sensitivity to the range increases with the source depth increasing. The time delay of B arrival shows to be highly sensitive to the source range increasing but insensitive to the source depth increasing.

As a result, the localization method combining the time delays of the S and B arrivals can achieve high resolution both in the depth direction and range direction and the source location can be estimated accurately.

However, if only the D, S, and B arrivals are used, the false peaks would appear in the ambiguity surface as the source location cannot be determined uniquely by a pair of time delays. For example, if the time delays are 0.2 ms and 0.05 ms the source locations can be 23 km in range and 690 m in depth or 13 km in range and 130 m in depth. The former is right when the time delay of S arrival is 0.2 ms. The latter is right when the time delay of B arrival is 0.2 ms. More arrivals are required to eliminate the false peaks. However, the other arrivals suffer scattering from the boundaries many times and are thus weak and unstable. An alternative method is to use the arrival angle information to identify the false peaks.

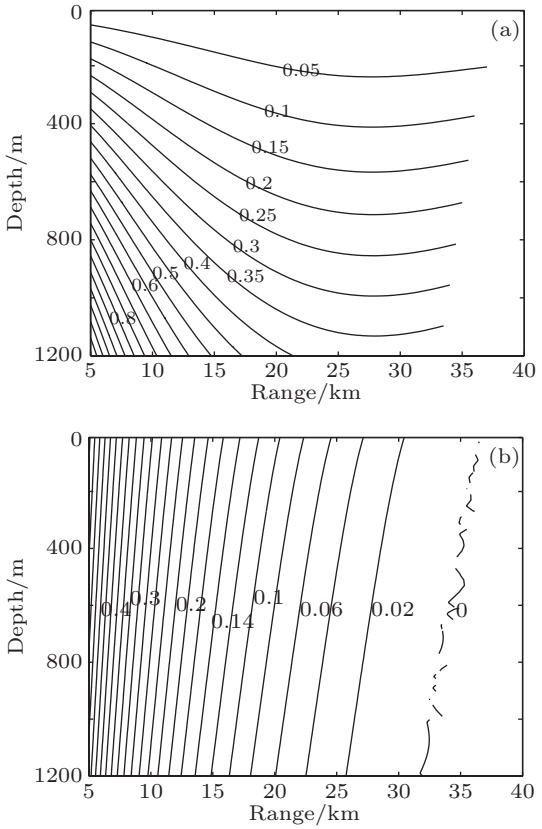


Fig. 7. Contours of time delays on a receiver of 4450 m for the cases of (a) the surface-reflected arrival and (b) the bottom-reflected arrival.

For the passive localization, as the signal waveform is not known, the methods of estimating the time delay are rather complicated such as blind deconvolution[22] and cepstrum.[23] A general method is to extract the time delay from the signal autocorrelation. However, the time resolution is inversely proportional to the bandwidth of the signal. Therefore, the method is not suitable for the narrowband signal. A simple and direct method is given in Ref. [18], which is based on the waveform estimation and the cross-correlation method. However, as the time interval between arrival groups in Fig. 4 is several seconds, the sampling time must be several seconds to obtain the time delay. Furthermore, the correlations between the multipath arrivals would be weak due to the scattering effect of the boundaries. Therefore, in the limited

sampling time the source localization method based on time delays is not effective in the RAP environment. In contrast, the arrival angles can be estimated in the relatively short sampling time and the correlations between the arrivals are not required, so the method based on the arrival angles is more feasible in the RAP environment.

3. Source localization method in RAP environment

As it is noted in Subsubsection 2.2.2, the time delays of multipath arrivals are hard to estimate with narrowband signal, especially when the sample time is limited the source localization method based on arrival angles is feasible in the RAP environment. However, as the multipath arrival angles can be very close to each other, the estimation of the arrival angle is complicated and inaccurate. In this section, a new method is presented for the RAP environment. The method stems from the WSF method, which is used to the estimation of direction of arrival.[21] The theory for plane waves can be seen in Ref. [21]. In the present paper, combing the WSF method and the matched-field theory a new method is presented.

3.1. WSF-MF method

Let an array of M elements receive D narrowband plane waves with arrival angles $\boldsymbol{\theta}_0$ being $[\theta_1, \theta_2, \ldots, \theta_d, \cdots, \theta_D]^{\mathrm{T}}$, where θ_d is the arrival angle of the d-th arrival, then, the array outputs will be

$$\boldsymbol{x}(t) = \boldsymbol{A}(\boldsymbol{\theta}_0)\boldsymbol{s}(t) + \boldsymbol{n}(t), \tag{1}$$

where, the array manifold $\boldsymbol{A}(\boldsymbol{\theta}_0)$ is an $M \times D$ matrix whose d-th column $\boldsymbol{a}(\theta_d)$ is the steering vector for the d-th arrival; D-vector $\boldsymbol{s}(t)$ is the complex signals; $\boldsymbol{n}(t)$ is the additive noise and assumed to be a stationary, zero-mean, Gaussian process and it is uncorrelated with the signals. The WSF method is that the arrival angle $\boldsymbol{\theta}_0$ can be estimated by minimizing the distance between the signal subspace and the spanned space by the array manifold

$$\tilde{\boldsymbol{\theta}}_0 = \min \left\| \boldsymbol{U}_{\mathrm{s}} \boldsymbol{W}^{1/2} - \boldsymbol{A}(\boldsymbol{\theta})\boldsymbol{T} \right\|_{\mathrm{F}}^2, \tag{2}$$

where $\|\bullet\|_{\mathrm{F}}$ denotes the Frobenius norm $\boldsymbol{U}_{\mathrm{s}}$ is the signal subspace given by the eigendecompostion of the array covariance $\boldsymbol{R}_{\boldsymbol{x}}$

$$\boldsymbol{R}_x = E(\boldsymbol{x}(t)\boldsymbol{x}^H(t)) = \boldsymbol{U}_{\mathrm{s}}\boldsymbol{\Lambda}_{\mathrm{s}}\boldsymbol{U}_{\mathrm{s}}^H + \sigma^2\boldsymbol{U}_n\boldsymbol{U}_n^H. \tag{3}$$

Here, diagonal matrix $\boldsymbol{\Lambda}_{\mathrm{s}}$ contains the D' largest eigenvalues the columns of the $\boldsymbol{U}_{\mathrm{s}}$ are the corresponding eigenvectors, σ^2 is the variance of the noise and the noise subspace $\boldsymbol{U}_n$ contains the M–D' eigenvectors. In Eq. (2), $\boldsymbol{W}$ is a positive-definite weighting matrix. To give the lowest asymptotic variance, $\boldsymbol{W}$ equals $\boldsymbol{\Lambda}^2\boldsymbol{\Lambda}_{\mathrm{s}}^{-1}$, where $\boldsymbol{\Lambda}$ is $\boldsymbol{\Lambda}_{\mathrm{s}}$–$\sigma^2\boldsymbol{I}$. Solving Eq. (2) for $\boldsymbol{T}$ and substituting back into Eq. (2), one obtains

$$\tilde{\boldsymbol{\theta}}_0 = \min \mathrm{tr}\{P_{\boldsymbol{A}}^{\perp}(\boldsymbol{\theta})\boldsymbol{U}_{\mathrm{s}}\boldsymbol{W}\boldsymbol{U}_{\mathrm{s}}^H\}, \tag{4}$$

where $P_{\boldsymbol{A}}^{\perp}(\boldsymbol{\theta}) = \boldsymbol{I} - P_{\boldsymbol{A}} = \boldsymbol{I} - \boldsymbol{A}\boldsymbol{A}^{\dagger} = \boldsymbol{I} - \boldsymbol{A}(\boldsymbol{A}^H\boldsymbol{A})^{-1}\boldsymbol{A}^H$. Here, $\boldsymbol{A}$ is the array manifold in Eq. (2).

In the RAP environment, it is assumed that the array aperture is rather small and the source is in the far field. Therefore, the D multipath arrivals can be approximately modeled as D plane wave. It is noted that the D multipath arrivals are correlated, thus the rank of signal subspace D' may be smaller than D. The WSF method is still valid in this condition, so equation (4) can be solved by the iteration method to estimate the arrival angles of the multipath arrivals. However, the initial angle has a significant influence on the result and thus must be estimated by using another method such as MUSIC. It imposes a great limitation on the application of the method, especially in the case of multipath detection problem, where the resolution of MUSIC is not high enough to distinguish the multipath arrival angles in many cases.

It is noted that the source localization is different from the multi-source detection in the sense that source location is restricted in a finite range-depth space just as the MFP problem. Therefore, the source location can be directly estimated in the range-depth space with no need for estimating the arrival angles beforehand. It is assumed that the array receives the multipath signals from a hypothesized source, whose location is denoted by $\boldsymbol{\psi}_{\mathrm{h}}$= [$z$,$r$] where z is the source depth from the ocean surface and r is the horizontal range from the array. The arrival angles of the multipath arrivals on the array each are a function of hypothesized source location, i.e.,

$$\boldsymbol{\theta}_{\mathrm{h}} = f(\boldsymbol{\psi}_{\mathrm{h}}), \tag{5}$$

where function $f(\bullet)$ is determined by the acoustic environment and can be calculated by standard ray approach. Substituting Eq. (5) into Eq. (4), one obtains

$$\tilde{\boldsymbol{\psi}}_0 = \min \mathrm{tr}\{P_{\boldsymbol{A}}^{\perp}(f(\boldsymbol{\psi}_{\mathrm{h}}))\boldsymbol{U}_{\mathrm{s}}\boldsymbol{W}\boldsymbol{U}_{\mathrm{s}}^H\}, \tag{6}$$

where $\tilde{\boldsymbol{\psi}}_0$ is the estimated source location. As it has been pointed out that the space of the source location is finite, the estimated source location $\tilde{\boldsymbol{\psi}}_0$ can be given by searching the range-depth space of the source location to satisfy Eq. (6). Considering the features of the multipath arrival, equation (6) can be modified to improve its performance. If the arrival angles are different, $\boldsymbol{A}$ is full. However, some multipath arrival angles may be so close that if the singular value decomposition (SVD) is applied to $\boldsymbol{A}$, some singular values are significantly smaller than the largest one. It means that the projections of the components of $\boldsymbol{A}$ on the subspace corresponding to the small singular values are very small. As the estimated signal subspace $\boldsymbol{U}_{\rm s}$ is not accurate, it may not represent the subspace corresponding to the small singular values in the real environment. To improve the performance of the localization, a reduced $\boldsymbol{A}$ can be used. $\boldsymbol{A}$ can be given by the SVD decomposition,

$$\boldsymbol{A} = \sum_{i=1}^{D} \boldsymbol{g}_i \sigma_i \boldsymbol{v}_i, \tag{7}$$

where $\boldsymbol{G} = [\boldsymbol{g}_1, \boldsymbol{g}_2, \ldots, \boldsymbol{g}_D, \ldots, \boldsymbol{g}_M]$ and $\boldsymbol{V} = [\boldsymbol{v}_1, \boldsymbol{v}_2, \ldots, \boldsymbol{v}_D]$ are the unitary matrixes and σ_i is the i-th singular value. The first P singular values and the corresponding vectors are used to reduce $\boldsymbol{A}$,

$$\boldsymbol{A}_r = \sum_{i=1}^{P} \boldsymbol{g}_i \sigma_i \boldsymbol{v}_i. \tag{8}$$

Substituting Eq. (8) into Eq. (6), the WSF-MF method is given by

$$\tilde{\boldsymbol{\psi}}_0 = \min \mathrm{tr}\{P^{\perp}_{\boldsymbol{A}_r}(f(\boldsymbol{\psi}_{\rm h}))\tilde{\boldsymbol{U}}_{\rm s}\boldsymbol{W}\tilde{\boldsymbol{U}}_{\rm s}^{H}\}. \tag{9}$$

Equations (6) and (9) show that the arrival angles are the transient parameters and are not estimated. As a result, the WSF-MF method using Eq. (6) or Eq. (9) can work automatically unlike the conventional methods in which the arrival angles offline must be distinguished. Furthermore, in the deep ocean environment, the SSP varies only in the upper ocean. Therefore, to reduce the computational cost of Eqs. (6) and (9), $f(\bullet)$ can be obtained by the standard ray approach beforehand through using the averaged SSP rather than the observed SSP.

The energy spectrum of the source locations corresponding to the WSF-MF method is defined as

$$E_{\rm WSF} = \frac{1}{\mathrm{tr}\{P^{\perp}_{\boldsymbol{A}_r}(f(\boldsymbol{\psi}_{\rm h}))\tilde{\boldsymbol{U}}_{\rm s}\boldsymbol{W}\tilde{\boldsymbol{U}}_{\rm s}^{H}\}}. \tag{10}$$

In an ideal environment, when the hypothesized source location $\boldsymbol{\psi}_{\rm h}$ coincides with the real source location, the denominator would be zero and thus the power output is infinite. In contrast, if $\boldsymbol{\psi}_{\rm h}$ deviates from the real source location greatly, the energy can be very small. Therefore, the energy spectrum is a high-resolution function. The normalized spectrum (ambiguity surface) in dB is defined as

$$E_{\rm N} = 10\log_{10}\left(\frac{E_{\rm WSF}}{\max(E_{\rm WSF})}\right) \quad \mathrm{dB}, \tag{11}$$

3.2. Features of the WSF-MF method

From the acoustic properties of the RAP environment and the theoretical basis of the WSF-MF method, the features are summarized as follows.

(i) This method uses the information about multipath arrival angles indirectly. Based on the ray propagation model, the arrival angle in Eq. (4) is substituted by the source location (see Eq. (6)). Therefore, the complicated estimation of the arrival angles is avoided.

(ii) As summarized in Subsubsection 2.2.2, the source location can be determined uniquely by the arrival angles of the D, S, and B arrivals, so the ambiguity surface of the WSF-MF method would not have false peaks.

(iii) The array for the WSF-MF method is relatively short. As the WSF-MF method is based on the WSF method, which is a high-resolution method for arrival angles, the long array for the matched-field method is not required any more.

(iv) The information about the time delays is not used in the WSF-MF method. The estimation of the time delays is difficult under the passive localization of a narrowband source.

These features make the WSF-MF applicable for the passive localization in the RAP environment and are verified in the following section.

4. Performance study of the WSF-MF method

In this section, simulations are conducted to study the performance of the WSF-MF method in the RAP environment. The environment is the same as that for the simulations in Section 2. The array is below the critical depth with the topmost element being at 4400 m. The array space is half the wavelength.

To simulate the signals on the array, the amplitudes, arrival angles and time delays of the eigenrays from the source to all the elements are calculated. The arrivals with three or more bounces on the sea surface and the sea bottom are omitted as these arrivals are weak for the scattering effects of the surface and the bottom. The arrivals are summed to obtain the composite signal at the elements. As the signals and the noises on the elements are narrowband Gaussian stochastic process, the SNR is given by

$$\mathrm{SNR} = 10\log_{10}(\sigma_{\mathrm{s}}^2/\sigma_{\mathrm{n}}^2), \tag{12}$$

where, σ_{s}^2 and σ_{n}^2 are the mean variances of the signals and the noises on the elements. Finally, the received signal is composed of the composite signal and the additive noise under an SNR. The sample frequency is 4 kHz and the sampling time is 2 s. The central frequency of the source signal is 300 Hz.

It must be pointed out that the WSF-MF method is derived on the assumption that the multipath arrivals on the array are plane waves. In reality, it is not the case. The received signals simulated by the above method would give rise to the mismatch between the simulated multipath arrivals and the plane waves (the mismatch is called plane-wave mismatch). As a result, it brings an error to the WSF-MF method which cannot be corrected by increasing the SNR or the array length.

In this section, the effects of SNR and element number (array aperture) on the performance of the WSF-MF method are analysed. Then the sensitivity to the the SSP mismatch is analysed to illustrate the robustness of the WSF-MF method.

4.1. Effects of SNR

In this section, the element number is fixed to be 16. The source is placed at 210 m in depth and 30 km in range. The replica fields are computed from 1 m to 121 m in depth at 20-m interval and from 5 km to 40 km in range at 0.5 km interval. Under the SNRs of 30 dB and 10 dB, the ambiguity surfaces for the source using the WSF-MF method are shown in Figs. 8(a) and 8(b), respectively. Figure 8 illustrates three features of the WSF-MF method.

i) The ambiguity surfaces each have a peak value (denoted by the white square in Fig. 8) around the real source location. Therefore, it is a valid method for source localization in the RAP environment. Figure 8(a) shows that the peak value is at 250 m in depth and 30 km in range which is very close to the real source location. The normalized power at the source location is −2.03 dB. To find the reason for the error, simulation is conducted under the plane waves. The peak is right at the source location in Fig. 8(c), which demonstrates that the error results from the plane-wave mismatch.

ii) The ambiguity surface of the WSF-MF method does not have false peaks in the RAP environment. It is stemmed from the fact that in Subsection 2.2 the arrival angles at other grids are significantly different from those at the grids around the source location.

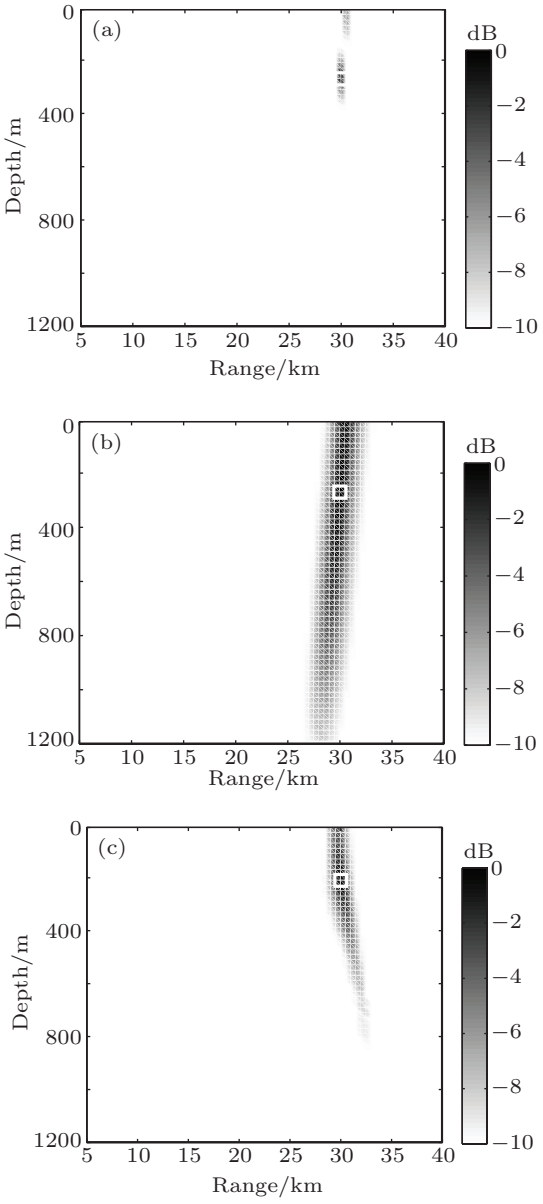


Fig. 8. Ambiguity surfaces for a source at 210 m in depth and 30 km in range using an array of 16 elements based on the WSF-MF method, in the cases, i.e. when SNRs are 30 dB (a), 10 dB (b), and when the environment is ideal, i.e., without plane-wave mismatch (c).

iii) As the WSF method can suppress the noise effectively and can work in the relatively low SNR, the WSF-MF method can also work in a relatively low SNR condition. However, the resolution would decrease with the decrease of the SNR especially in the depth direction. Figure 8(b) shows that all the grids at the depth from 10 m to 500 m and around 30 km in range have large power and thus the error of the source localization may appear in the depth.

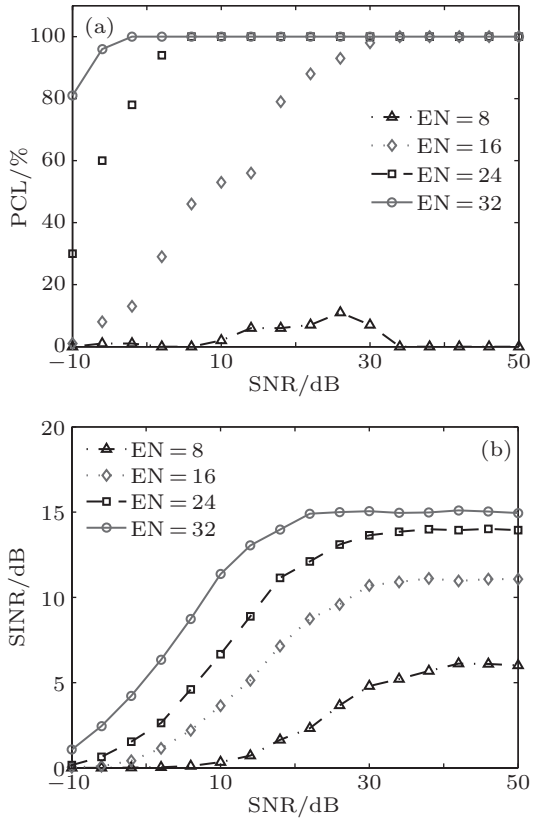


Fig. 9. Curves of probability of correct localization (PCL) (a) and signal-to-interference noise ratio (SINR) (b) versus signal-to-noise ratio (SNR), obtained from the WSF-MF method, element is abbreviated as EN.

To illustrate the SNR effects on the WSF-MF method fully, a quantitative measure of the source localization performance, probability of correct localization (PCL) is presented in Fig. 9(a). The localization is right if the computed source location is within 40 m in depth and 0.5 km in range of the actual source location. Furthermore, to show the resolution of the WSF-MF method, the signal-to-interference noise ratio (SINR) is defined as,

$$\mathrm{SINR} = 10\log_{10}\left(\frac{1/\operatorname{tr}\{P_A^{\perp}(f(\boldsymbol{\psi}_0))\tilde{\boldsymbol{U}}_{\mathrm{s}}\boldsymbol{W}\tilde{\boldsymbol{U}}_{\mathrm{s}}^H\}}{m\{1/\operatorname{tr}\{P_A^{\perp}(f(\boldsymbol{\psi}))\tilde{\boldsymbol{U}}_{\mathrm{s}}\boldsymbol{W}\tilde{\boldsymbol{U}}_{\mathrm{s}}^H\}\}_{\mathrm{rect}}}\right), \quad (13)$$

where $m\{\bullet\}$ is the mean operator. The numerator is the power output (see Eq. (10)) at the source location and the denominator is the mean power output in a rectangular search space covering the source location. According to the definition, a higher SINR indicates that the mainlobe is sharper. The SINR as a function of SNR is shown in Fig. 9(b), where the rectangular search space is from 10 m to 510 m in depth and 28 km to 32 km in range. Under an array of 8 elements, no matter how high the SNR is, the localization is unsuccessful. Under an array of 32 elements, the PCL reaches 100% at −2 dB SNR while the resolution keeps increasing until the SNR is 25 dB. Figure 9 shows that the SNR has significant influence on the performance of the WSF-MF method especially for a short array (e.g., 16 elements).

4.2. Effects of array length

In general, the source localization based on the arrival structure needs to consider both the resolution of the arrival angles and the plane-wave mismatch, so the array length is a compromise between the two factors. The compromise is determined by the acoustic environment. Under the RAP environment shown in Fig. 1(a), the arrival time of multipath arrivals varying with depth is shown in Fig. 10, where the time delay relative to the arrival time at 4300-m deep is given. The source is placed at 210 m in depth and 30 km in range. The D, S, B, and SB arrivals impinge on the array from the bottom direction, so the time delays are negative. In contrast, the BS arrival is from the surface direction, so the time delays are positive.

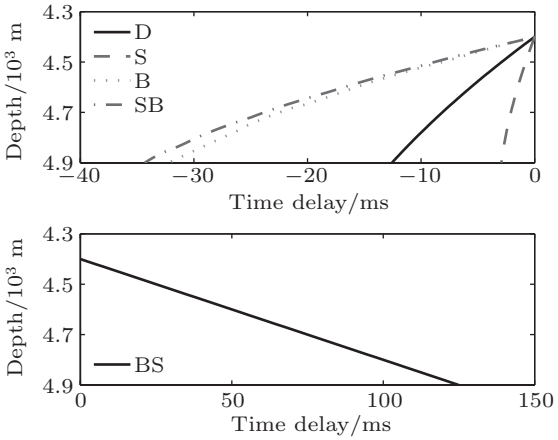


Fig. 10. Curves of depth versus time delay relative to the arrival time at 4300-m deep under the source 210 m in depth and 30 km in range.

Figure 10 shows that the curves of the depth versus time delay are not straight lines, which does not

accord with the case of plane wave. However, if the array is not too long and not placed near the bottom either, the curves of time delay are approximately straight lines especially for the BS arrival. Under this condition, it is expected that the performance of the WSF-MF method would be better for a longer array. The ambiguity surface of the WSF-MF method using an array of 32 elements is shown in Fig. 11, where the other condition is the same as that in Fig. 8(b). Compared with Fig. 8(b), the resolution in Fig. 11 is much higher. Another example is shown in Fig. 12 where the element number is 8 and the SNR is 30 dB. No highlight near the source location can be observed in the ambiguity surface and the peak value is at 10 m in depth and 30.5 km in range. Comparing Fig. 11 with Fig. 8(a), it is obvious that under the high SNR, the array length would also influence the performance of the WSF-MF significantly.

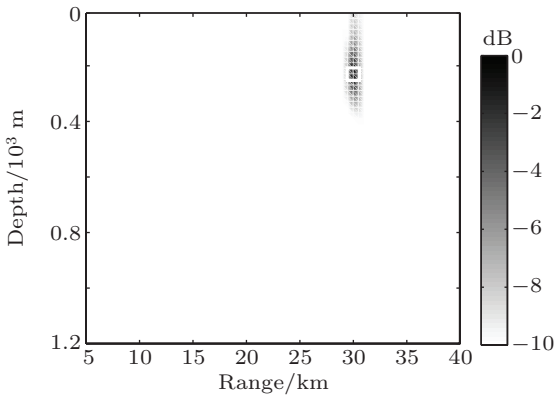


Fig. 11. Ambiguity surfaces for a source at 210 m in depth and 30 km in range using an array of 32 elements based on the WSF-MF method. The SNR is 10 dB.

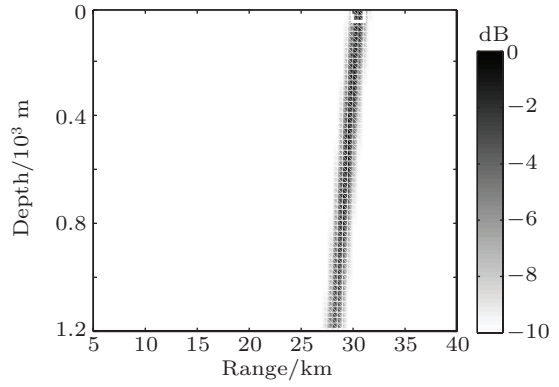


Fig. 12. Ambiguity surfaces for a source at 210 m in depth and 30 km in range using an array of 8 elements based on the WSF-MF method. The SNR is 30 dB.

The curves of PCL and the SINR (see Eq. (13)) versus element number for the WSF-MF method are displayed in Fig. 13. The PCL curves indicate that an array with more than 30 elements can work under the SNR above 0 dB. The curves of SINR demonstrate that when the element number is small (below 35 in Fig. 13(b)) the resolution quickly increases and if the element number is large (above 60 in Fig. 13) the resolution gradually decreases. The decrease results from the plane-wave mismatch as the array aperture is enlarged. Under the low SNR (0 dB), the resolution keeps increasing until the element number reaches 60. It indicates that a larger array is required to work in the lower SNR environment.

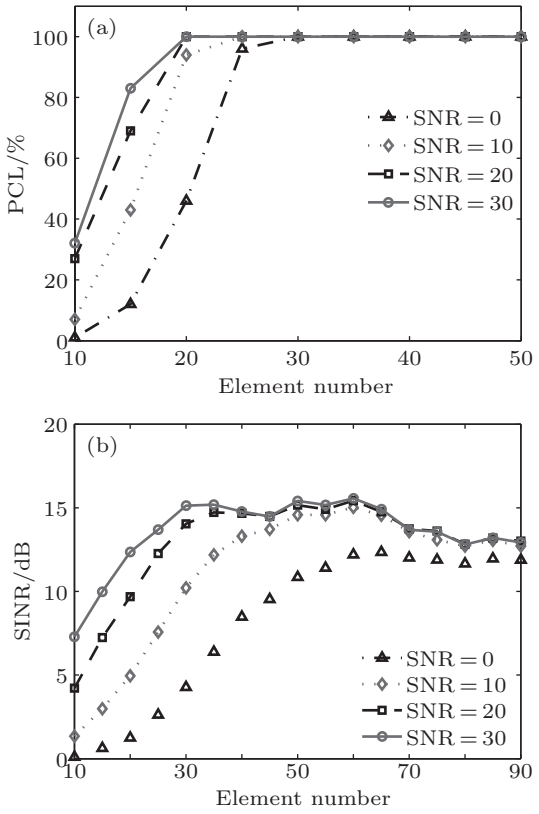


Fig. 13. Curves of probability of correct localization (PCL) (a) and signal-to-interference noise ratio (SINR) (b) versus element number, obtained from the WSF-MF method.

Above all, the array length is one of the factors determining the performance of the WSF-MF method. The array cannot be too long in order to avoid the plane-wave mismatch. The requirement for the array length would be more rigid under lower SNR. In the RAP environment, the ambient noise level is rather low and thus the SNR is high, so a relatively short array can work. An array with 32 elements has a good performance when the SNR is above 0 dB and thus it can work in the RAP environment.

4.3. Sensitivity to the SSP mismatch

The source localization by means of matched-field method or the ray approach is known to be sensitive to the environmental parameters, such as SSP, sediment and bottom properties, sea surface roughness, etc.[24] In a real environment, the SSP changes with time and range and thus the mismatch between the real SSP and the SSP for the replica field calculation always exists. In this part, the performance of the WSF-MF method is analysed in an environment with SSP mismatch.

As is well known the SSP is stable in the deep ocean. The SSP mismatch is mainly due to the variation of the SSP in the upper ocean.[24] In the present paper the SSP for calculating the measurement field is the same as that shown in Fig. 1(a) and the SSP for the replica field is simulated by the empirical-orthonormal-function (EOF) technique.[25] The SSP can be expressed as the sum of the mean SSP and the weighted EOFs,

$$c(z) = c_0(z) + \sum_{k=1}^{K} \alpha_k g_k(z), \tag{14}$$

where $c_0(z)$ is the mean SSP, $g_k(z)$ is the k-th EOF, and α_k is the corresponding coefficient. The mean SSP is the one shown in Fig. 1(a). The EOFs are calculated using the SSP samples around (0° E, 0° N) from the year 2002 to 2007, where the water depth is about 5000 m. The ranges of the EOF coefficients are calculated at the same time. The SSP samples are obtained from the Simple Ocean Data Assimilation (SODA)[26] dataset. A set of randomly perturbed SSP is simulated by substituting the coefficients of Eq. (14) with random values from the ranges of the EOF coefficients. The root-mean-square (RMS) error of these SSPs as a function of depth is shown in Fig. 14, where the RMS error is given by

$$\mathrm{RMS}_d = \sqrt{\frac{1}{N}\sum_{i=1}^{N}\left|c(z_{i,d}) - \overline{c(z_d)}\right|^2}, \tag{15}$$

where N is the number of the perturbed SSPs, $c(z_{i,d})$ is the sound speed of the i-th perturbed SSP at the d-th depth grid, and $\overline{c(z_d)}$ is the sound speed of the mean SSP at the d-th depth grid. The RMS errors from 0 m to 150 m deep are large, which demonstrates the SSP variation in the upper ocean.

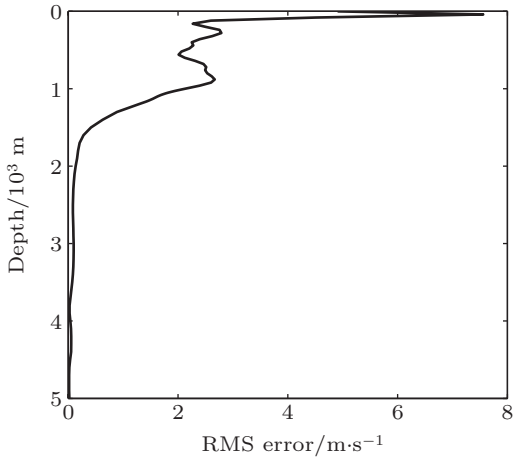


Fig. 14. Root-mean-square error of the simulated sound speed profiles versus depth.

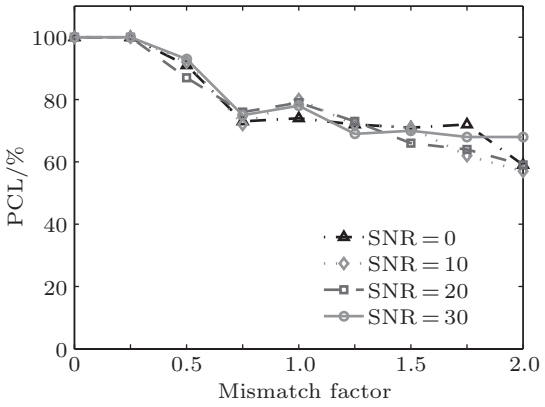


Fig. 15. Curves of PCL versus mismatch factor under different SNRs.

An array with 32 elements is used to localize the source at 210 m in depth and 30 km in range. To quantify the SSP mismatch, the range of the EOF coefficient is multiplied by a factor called mismatch factor. The larger the mismatch factor, the more significant the mismatch is. Under different SNRs, the PCLs of WSF-MF method versus mismatch factor are displayed in Fig. 15, showing that the performance of the WSF-MF method deteriorates gradually as mismatch factor increases. The increase of the SNR cannot improve the robustness of the WSF-MF method when the SNR is higher than 0 dB. To compare the robustness of the WSF-MF method with that of the Bartlett matched-field processor[27] which is subjected to high sidelobes but is robust in the uncertain environment, the PCLs under 0 dB are shown in Fig. 16, indicating that the WSF-MF is more robust than the Bartlett method in the RAP environment. It is because that the array aperture is small and thus the spatial sample

length is not enough for the Bartlett method. Therefore, the Bartlett method is more sensitive to the SSP variation. For the WSF-MF method, the robustness results from the large take-off angles of the multipath arrivals from the source. Snell's law indicates that the ray with large grazing angle is insensitive to the variation of the sound speed. The WSF-MF method makes full use of the arrival angles and thus it is robust in this environment.

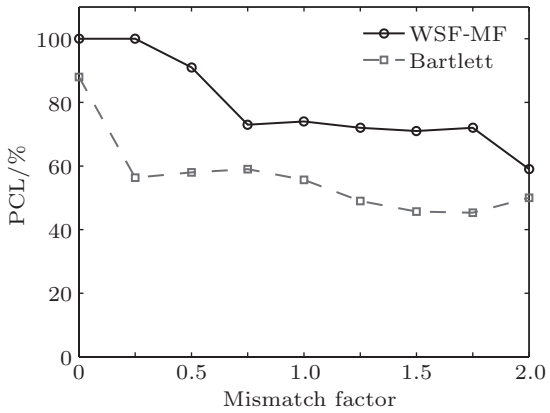


Fig. 16. Curves of PCL versus mismatch factor based on the WSF-MF method and the Bartlett matched-field processor.

In the SSP mismatch environment, the peak of the ambiguity surface may deviate from the real location. To quantify this error, the RMS error of the localization is defined as,

$$\mathrm{RMS}_{\mathrm{Depth}} = \sqrt{\frac{1}{N}\sum_{i=1}^{N}|z_i - z_r|^2}, \tag{16}$$

$$\mathrm{RMS}_{\mathrm{Range}} = \sqrt{\frac{1}{N}\sum_{i=1}^{N}|r_i - r_r|^2}, \tag{17}$$

where $\mathrm{RMS}_{\mathrm{Depth}}$ and $\mathrm{RMS}_{\mathrm{Range}}$ are the RMS errors of the depth and range, respectively; N denotes the number of the simulation; z_i and r_i are the estimated source depth and range for the i-th simulation, respectively; z_r and r_r are the real source depth and range, respectively. Under the SNR of 0 dB, the RMS errors changing with the mismatch factor are shown in Table 1. Generally, the depth RMS errors increase with the mismatch factor increasing, while the range RMS errors are within 0.5 km for all mismatch factors. The maximum depth RMS error is 104 m while the maximum range RMS error is about 1 percent of the real source range. In conclusion, the estimated source location does not deviate from the real source location very far, especially in the range direction.

Table 1. RMS errors of the localization under different SSP mismatches.

Mismatch factor	Depth RMS error/m	Range RMS error/km
0.00	17	0.00
0.25	21	0.05
0.50	29	0.05
0.75	73	0.35
1.00	94	0.42
1.25	83	0.32
1.50	80	0.36
1.75	82	0.34
2.00	104	0.29

5. Conclusions

In this paper, the acoustic properties of the RAP are analysed in detail and based on its characteristics a WSF-MF method for the source localization using the multipath arrival angles is presented. Four characteristics of the RAP environment are as follows. First, the RAP is the direct path between the source and the receiver and thus is insensitive to the surface scattering and the bottom reflection loss. Second, when the array is placed below the critical depth the ambient noise is much lower than that on the array above the critical depth. Third, in the medium range, when the RAP is used for surveillance, it does not have blind zone. Finally, for the passive narrowband source localization, the methods based on the arrival angles have higher resolutions in the range direction than that in the depth direction. The simulations of the WSF-MF method are consistent with this conclusion. The methods based on the time delays of multipath arrivals have high resolutions both in range direction and in depth direction but it is not applicable for the RAP environment.

The WSF-MF method is derived for using a short array in the deep ocean and avoiding the complicated estimation of the arrival angles at the same time. This method combines the efficient ray propagation model with the signal processing technique to accomplish the source location in a finite range-depth space rather than the arrival angle space. Some key advantages of the method when it is used in the RAP environment are summarized as follows. First, the ambiguity surface of the WSF-MF method does not have false peaks. However, the width of the peak increases with the decrease of SNR or array length. Second, the source localization can be done with relatively short arrays by using the WSF-MF method. An array with 32 el-

ements in which the spacing between two elements is half the wavelength has good performance when the SNR is above 0 dB. Finally, the WSF-MF method is more insensitive to the variation of the sound speed than the Bartlett matched-field processor.

As the deep ocean array is not available, the results in this paper cannot be verified at present. It is hoped that the physical properties of the RAP and the WSF-MF method can be verified experimentally in the future.

References

[1] Baggeroer A B, Scheer E K, Heaney K, Spain G D, Worcester P and Dzieciuch M 2010 *J. Acoust. Soc. Am.* **128** 2385

[2] Zurk L M 2009 *J. Acoust. Soc. Am.* **125** 2576

[3] Heaney K D, Campbell R C, Baggeroer A B, Gerald L, Worcester P and Dzieciuch M A 2010 *J. Acoust. Soc. Am.* **128** 2386

[4] Urick R J 1983 *Principles of Underwater Sound* 3rd edn. (New York: McGraw-Hill)

[5] Gaul R D, Knobles D P, Shooter J A and Wittenborn A F 2007 *IEEE J. Oceanic Eng.* **32** 497

[6] Westwood E K 1992 *J. Acoust. Soc. Am.* **91** 2777

[7] Thompson S R 2009 *Sound Propagation Considerations for a Deep-Ocean Acoustic Network*, DTIC Document

[8] Zhang T W, Yang K D and Ma Y L 2010 *Chin. Phys.* B **19** 124301

[9] Lei B, Yang K D and Ma Y L 2010 *Chin. Phys.* B **19** 054301

[10] Porter M, Dicus R and Fizell R 1987 *IEEE J. Oceanic Eng.* **12** 173

[11] Tantum S L, Nolte L W and Wazenski M T 1998 *J. Acoust. Soc. Am.* **104** 1809

[12] Wang N and Liu J Z 2002 *Chin. Phys.* **11** 456

[13] Yang T C 1990 *J. Acoust. Soc. Am.* **87** 2072

[14] Baggeroer A B and Kuperman W A 1992 *J. Acoust. Soc. Am.* **91** 2422

[15] Abel J S and Smith J O 1989 *IEEE Trans. Acoust. Speech Signal* **37** 1157

[16] Collins M D and Kuperman W 1991 *J. Acoust. Soc. Am.* **90** 1410

[17] Sun Z G, Ma Y L, Tu Q P and Jiang X Q 1997 *Chinese Journal of Acoustics* **16** 3

[18] Voltz P and Lu I T 1994 *J. Acoust. Soc. Am.* **95** 805

[19] Ma J, Gao C and Tan L Y 2007 *Chin. Phys.* **16** 1327

[20] Zhao X F and Huang S X 2011 *Chin. Phys.* B **20** 029201

[21] Viberg M, Ottersten B and Kailath T 1991 *IEEE Trans. Signal Process.* **39** 2436

[22] Yan S F and Ma Y L 2004 *Journal of Electronics and Information Technology* **26** 702

[23] Stéphenne A and Champagne B 1997 *Signal Processing* **59** 253

[24] Tolstoy A 1989 *J. Acoust. Soc. Am.* **85** 2394

[25] Zhang Z B, Ma Y L, Yang K D and Yan S F 2004 *Chinese Journal of Acoustics* **23** 259

[26] Carton J A, Chepurin G, Cao X and Giese B 2000 *J. Phys. Oceanogr.* **30** 294

[27] Baggeroer A B, Kuperman W A and Mikhalevsky P N 1993 *IEEE J. Oceanic Eng.* **18** 401